Making Nonwoven Fibrous Poly(ε-caprolactone) Constructs for Antimicrobial and Tissue Engineering Applications by Pressurized Melt Gyration

Zewen Xu, Sunthar Mahalingam, Pooja Basnett, Bahijja Raimi-Abraham, Ipsita Roy, Duncan Craig, Mohan Edirisinghe*

A pressurized melt gyration process has been used for the first time to generate poly(ε-caprolactone) (PCL) fibers. Gyration speed, working pressure, and melt temperature are varied and these parameters influence the fiber diameter and the temperature enabled changing the surface morphology of the fibers. Two types of nonwoven PCL fiber constructs are prepared. First, Ag-doped PCL is studied for antibacterial activity using Gram-negative *Escherichia coli* and *Pseudomonas aeruginosa* microorganisms. The melt temperature used to make these constructs significantly influences antibacterial activity. Neat PCL nonwoven scaffolds are also prepared and their potential for application in muscular tissue engineering is studied with myoblast cells. Results show significant cell attachment, growth, and proliferation of cells on the scaffolds.

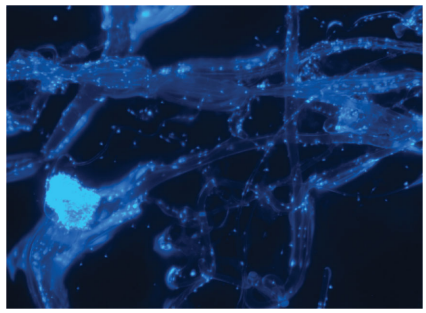

1. Introduction

Polymeric fibers have widely been used to construct porous polymer scaffolds in the form of woven and nonwoven scaffolds.[1,2] Generally, nonwoven polymer fibrous scaffolds are made with spinning techniques either using polymer solutions or melts.[3,4] The primary focus of the spinning technique is the production of fibers in a scale range from nano- to microrange that resembles the native extracellular matrix (ECM).[5–7] Although there has been much research on solution spinning to form fibrous polymer scaffolds for tissue engineering and wound healing applications, little has been reported on melt spinning to fabricate nonwoven scaffolds.[8,9] Melt spinning does not require solvents that are mostly cytotoxic, therefore it offers a distinct advantage. In addition, the surface topography of the fibrous scaffolds which can affect cellular infiltration can be better controlled by melt spinning.[8,10]

Poly(ε-caprolactone) (PCL) is one of the most promising linear aliphatic polyesters used extensively in the biomedical field since it is biodegradable in an aqueous medium and biocompatible in biological applications. This semi-crystalline polymer has a low melting point (60 °C) and a glass transition temperature (−60 °C) and therefore it could be fabricated easily into any shape and size.[11–13] The superior rheological properties and mechanical properties of PCL have

Z. Xu, Dr. S. Mahalingam, Dr. M. Edirisinghe
Department of Mechanical Engineering
University College London
London WC1E 7JE, UK
E-mail: m.edirisinghe@ucl.ac.uk
Dr. P. Basnett, Prof. I. Roy
Department of Life Sciences
University of Westminster
London W1W 6UW, UK
Dr. B. Raimi-Abraham, Prof. D. Craig
School of Pharmacy
University College London
London WC1N 1AX, UK

DOI: 10.1002/mame.201600116

attracted interest in using this polymer in tissue engineering scaffolds, blood vessels, vascular grafts, and wound healing mats.[8,14,15] The ability to blend PCL with other natural polymers such as bacterial cellulose and cellulose acetate also makes it an excellent candidate for wound dressing scaffolds.[16,17] Functionalization of PCL with filler materials like nanoparticles has also shown a significant improvement in overall properties and thus shows its flexibility in processing various architectures from it.[18]

Recently, pressurized gyration which involves rotating a perforated pot containing a polymer solution at high speed has become a promising alternative method of spinning nanofibers and nanofibrous structures.[19,20] This technique has attracted a wide interest in the research community because it overcomes the limitations of other spinning methodologies and it has already been exploited to generate fibers, microbubbles, and capsules using polymer and protein solutions.[19–22] A high production rate, ease of production, and highly controlled fiber morphology are salient features of this technique.[19] Typical pressurized gyration consists of simultaneous centrifugal spinning and solution blowing where combination of centrifugal and dynamic fluid flow forces acts against the surface tension force to generate fibers. The process control parameters such as rotating speed and working pressure influence the fiber size, fiber size distribution, and the morphology.[19,21] Yield and the quality of the fibers are primarily influenced by polymer concentration and the evaporation rate of the solvent. However, conventional pressurized gyration is dependent on solvent usage and this can be a disadvantage in forming bioconstructs because of toxicity issues. In contrast, pressurized melt gyration (PMG), reported for the first time in this study, does not require solvents as it forms a polymer melt in a gyrating pot containing orifices on its surface. The pot temperature can be controlled and micrometer size fibers whose surface roughness could be tailored can be made and investigated for typical bioengineering applications such as antibacterial resistance and tissue engineering, as attempted in this work.

2. Experimental Section

2.1. Materials

Poly(ε-caprolactone) (PCL, $[C_6H_{10}O_2]_n$, Mn ≈ 80 000, density = 1.145 g mL^{-1}, melt index 1 g/10 min) was purchased from Sigma-Aldrich (Poole, UK) for the purpose of making PCL scaffolds. Silver (Ag) nanoparticle (particle size in a range 10–150 nm) suspended in an organic solvent triethylene glycol monomethyl ether was obtained from Sigma-Aldrich (Poole, UK) for preparing Ag-coated PCL scaffolds. All the reagents were used without further purification.

2.2. Fabrication of PCL and Ag Loaded PCL Scaffolds

PCL scaffolds were made using a custom-made melt pressurized gyration apparatus (Figure 1) contained within a Perspex enclosure. The rotating aluminum vessel had 20 orifices (each orifice is 0.5 mm diameter in size) on its face and had heating elements built on it. The temperature of the gyration vessel could be elevated upto 600 °C. The temperature was monitored and controlled using an in-situ thermocouple. The accuracy of the temperature measurement was ±5 °C. Before loading the PCL pellets on to the vessel a stable temperature was attained by heating the gyration vessel for 5 min at a specified temperature. This facilitated upkeep of temperature homogeneity across the vessel and stable spinning of PCL scaffolds. The maximum rotating speed and the working pressure of the melt pressurized gyration were 36 000 rpm and 0.3 MPa, respectively. In this work PCL scaffolds were obtained at four different temperatures (95, 125, 155, and 200 °C) at various rotating speeds and working pressures.

Ag-loaded PCL fibers were processed using Ag-coated PCL pellets spun at different temperatures. These were obtained by immersing and soaking the PCL pellets in Ag nanoparticle solution using organic solvent triethylene glycol monomethyl ether at the ambient temperature (≈23 °C) for 5 h. The melt spun Ag-loaded PCL scaffolds were also coated with Ag nanoparticles using the gyratory vessel rotating at a speed of 36 000 rpm. 0.01% (v/v) Ag nanoparticle solution was made using organic solvent triethylene glycol monomethyl ether and distilled water. A homogenous solution was obtained after magnetically stirring for 1 h at ambient conditions (temperature ≈23 °C and relative humidity ≈45%). After coating, the Ag-PCL scaffolds were dried in a desiccator before being used for evaluation of antibacterial properties.

2.3. Characterization of the Fibrous Scaffolds

A scanning electron microscope (SEM; FEI Helios) was used to characterize the surface morphology of the fibrous scaffolds. The

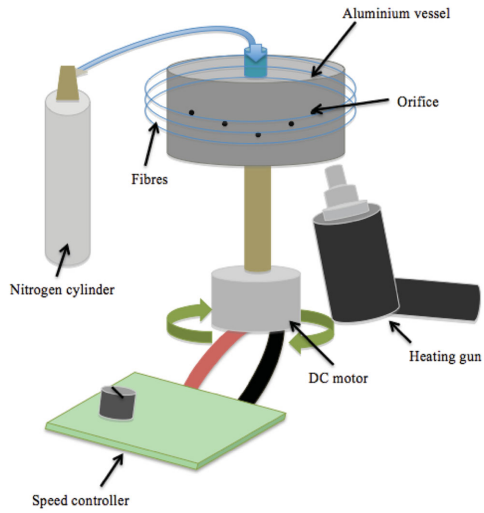

Figure 1. Experimental setup of melt-pressurized gyration process.

images were obtained with secondary electrons where PCL scaffolds were coated with gold using a sputtering machine (sputter time ≈75 s) before loading into the microscope. High- and low-magnification images were acquired at randomly selected positions (>20) within a sample. The fiber diameter was obtained using Image J software. About 150 measurements were made at random locations to plot the fiber diameter distribution. The scaffolds were also characterized using a fluorescence microscope (EVOS FL, Life Technologies) to verify the cell growth on the scaffolds.

Raman spectra of nylon and Ag-loaded nylon samples were obtained using a Renishaw Raman microscope excited with 514.5 nm incident wavelength radiation. The data acquisition covered the spectral range 3000–100 cm^{-1} with a spatial resolution of 4 cm^{-1}.

All differential scanning calorimetry (DSC) studies were conducted on a TA Instruments Q2000 unit (Newcastle, DE, USA) with a refrigerated cooling system attached and an accompanying dry nitrogen sample purge flow at 50 mL min^{-1}. Calibrations were performed using indium, *n*-octadecane, and tin; heat capacity constant calibration was performed using aluminium oxide TA sapphire disks at 2 °C min^{-1} with ±0.212 °C modulation amplitude over a 60 s period. All DSC experiments and calibrations were performed using a TA Instruments Tzero pan with an accompanying Tzero lid. Modulated temperature DSC (MTDSC) experiments were conducted on all samples (i.e., PCL starting material and PCL PMG fibers), heating at 2 °C min^{-1} with ±0.212 °C modulation amplitude over a 60 s period (over an appropriate temperature range). All experiments were conducted in triplicate. The data obtained were analyzed using the TA Instruments Universal Analysis 2000 software for Windows 2000/XP/Vista Version 4.7A.

UV/vis spectroscopy (Perkin Elmer) was used to study the Ag ion release from PCL-Ag composite fibrous mats. For this purpose, 100 mg of PCL-Ag mats spun at different temperatures were loaded into 10 mL deionized water and magnetically stirred at the ambient temperature. At a certain time interval 3 mL solutions were taken and analyzed in the wavelength range 300–700 nm. A PCL scaffold without Ag coating in deionized water was used as the control solution. Initially, a calibration curve was obtained for Ag ion concentrations and absorbance values. Various concentrations of Ag ion in deionized water were scanned in the wavelength range 300–700 nm and used to fit the calibration curve. This curve was used to measure the concentration (g L^{-1}) of Ag ion release in deionized water at a certain time interval.

2.4. Antibacterial Studies of Fibrous Scaffolds

Two Gram-negative bacteria, *E. coli* (in house strain number 3891, Centre for Clinical Science & Technology, UCL) and *P. aeruginosa* (strain 25-09071215-05) were used to investigate the antibacterial activities of PCL and Ag-coated PCL scaffolds. In this method, bacterial broth suspensions were cocultured under aerobic conditions with the sample for set periods of time, after which the number of viable colony-forming units (CFUs) of bacteria were obtained and then the antibacterial rate for each sample was calculated.

The assay was performed using bacteria cultured overnight from a single colony to stationary phase (≈10^9 CFU mL^{-1}) in Tryptic Soy Broth (TSB) in a shaking aerobic incubator kept at 37 °C. Next, a suspension, ≈5×10^5 CFU mL^{-1} in TSB, was prepared for use in the experimental bacterial suspension working in a sterile laminar flow hood environment.

Same weight of scaffold samples (0.04 g) was placed using sterile tweezers into each well of a 24-well tissue culture plate (Corning) along with 0.5 mL of the experimental bacterial suspension of either *E. coli or P. aeruginosa*. In these tests, eight samples spun at 36 000 rpm rotating speed were tested for each bacterium including four samples of PCL scaffolds produced at different temperatures (95, 125, 155, and 200 °C) and four samples of Ag-coated PCL scaffolds made at the same temperatures. Wells with experimental bacterial suspension alone containing no sample were also used as a negative control. The plates were cultured in an aerobic shaking incubator at 37 °C for 2 and 24 h. After coculturing with the samples, the bacterial suspensions were diluted (1:1, 1:10, 1:100, and 1:1000) into sterile tubes, after which 0.02 ml of each dilution was applied evenly onto quadrants of chromogenic agar plates (chromID CPS, Biomerieux) for enumeration using sterile L-spreaders. Chromogenic agar allows confirmation of bacterial species by colony colour. The plates were incubated at 37 °C for 24 h. Finally, the number of bacteria colonies (CFU) on each quadrant was counted to evaluate the effect of the original sample on survival of the bacteria. Culture medium without bacteria was used as a negative control. The antibacterial rate of the material can be determined by AR (%) = $[(N_1 - N_2)/N_1]$ x 100, where, AR is the antibacterial rate; N_1 is the bacterial count of the negative control and N_2 is the bacterial count of the antibacterial nanofibres.

2.5. In Vitro Biocompatibility Studies

2.5.1. C2C12 (Mouse Myoblast Cell Line) Culture

C2C12 cell line (mouse myoblast) was cultured using Dulbecco's Modified Eagle's Medium (DMEM) supplemented with 10% foetal calf serum, 1% penicillin, and 1% streptomycin solution in a 75 cm^2 tissue culture flask. Media was filtered, sterilized and warmed in a 37 °C water bath before use. Cells were cultured in a humidified atmosphere (5% CO_2, 95% air). Fresh media was added to the cells every 2 d. Cells were used for seeding the sterile fibrous scaffolds when they are confluent.

2.5.2. Cell Seeding on the Fibrous Scaffolds

The fibrous scaffolds were cut to 1 cm^2 to fit into the 24 well cell culture plates. They were sterilized using UV rays for 15 minutes. Prior to the seeding, the fibers were incubated overnight in DMEM at 37 °C. The confluent cells were trypsinized and recovered by centrifugation at 1000 rpm for 10 min. Cell pellet was thawed and fresh medium was added to the cell pellet. Cells were counted using a hemocytometer. A cell density of 25 000 cells was used to seed the fibrous scaffolds that were placed in 24 well plates. C2C12 cells were cultured on these fibrous scaffolds for 1, 3, and 7 d. Standard tissue culture plastic was used as the positive control for this experiment.

2.5.3. Cell Proliferation Assay

MTT assay (a colorimetric assay using tetrazolium dye MTT 3-(4, 5-dimethylthiazol-2-yl)-2, 5-diphenyltetrazolium bromide) was carried out to measure the cell viability at the end of each time point. MTT reagent was prepared by dissolving the reagent in phosphate buffered saline at a final concentration of 5 mg mL^{-1}. After the removal of the DMEM, 500 µL of MTT reagent was added to the scaffolds in the 24-well plate and incubated for 4 h at 37 °C. After the incubation was complete, MTT reagent was removed and 200 µL of dimethyl sulfoxide (used as a solubilizing agent) was added to the scaffolds and mixed thoroughly. It is well known that the viable cells with an active metabolism alter MTT reagent into a purple coloured formazan product with an absorbance maximum near 540 nm. Therefore, absorbance was measured at 540 nm using 96-well plate from Thermomax using Softmax Pro version 4.8 software. The following equation was used to calculate the % cell proliferation

$$\%\text{Cell Proliferation} = \frac{\text{Mean absorbance of samples}}{\text{Mean absorbance of control}} \times 100 \quad (1)$$

DMEM medium containing the cells in the tissue culture plastic was used as the positive control, whereas scaffolds incubated in the medium without the cells was used as the negative control.

3. Results and Discussion

PMG is a novel process that could provide a new pathway for solventless spinning of polymer fibers with high throughput. As shown in the high-speed camera video (Supporting Information), it involves melting a polymer in a rotating vessel and forcing the polymer melt through narrow orifices under the influence of centrifugal force and dynamic fluid flow. The molten polymer is subjected to a high vortex during the rotation where liquid jets eject from the orifices. When the withholding surface tension force that tends to restrict molten polymer flow is overcome by centrifugal force and dynamic fluid flow forces (due to pressurized gas) the ejection of the jets happens. The stretching of liquid jets are attenuated by centrifugal force in the rotating axis before rapid solidification of the fibers occur at collector around the vessel. The solidification of the fibers is also assisted by dynamic fluid flow through the orifice.

Table 1 shows fiber diameter variation with melt temperature. It is clearly seen that the fiber diameter reduces with increasing temperature. For PCL molten polymer, increasing the temperature from 95 to 200 °C reduced the fiber diameter from 38 to 28 µm at a rotating speed 24 000 rpm (Table 1a). At a rotating speed 36 000 rpm, increasing the temperature from 95 to 200 °C reduced the fiber diameter further, from 31 to 18 µm (Table 1a). Thus, the rotating speed of the vessel affects the fiber diameter, in addition to melt temperature. Table 1b show the variation of fiber diameter with melt temperature and working pressure. The fiber diameter reduced from 24 to 19 µm when increasing the temperature from 105 to 200 °C at a rotating speed 36 000 rpm and a working pressure 0.01 MPa. At a rotating speed 36 000 rpm and a working pressure 0.02 MPa, the fiber diameter reduced further, from 22 to 14 µm when increasing the temperature from 105 to 200 °C. This indicates that the working pressure had a significant influence on variation of the fiber diameter.

Table 1. PCL fiber diameter variations at various melt temperatures, rotating speeds, and working pressures: a) 24 000, 36 000 rpm with no pressure applied; b) 0.01, 0.02 MPa.

a)		
Sample	**Fiber diameter at 24 000 rpm [µm]**	**Fiber diameter at 36 000 rpm [µm]**
PCL 95 °C	38 ± 12	31 ± 7
PCL 125 °C	35 ± 15	26 ± 13
PCL 155 °C	31 ± 11	22 ± 12
PCL 200 °C	28 ± 10	18 ± 12
b)		
Sample	**Fiber diameter at 36 000 rpm and 0.01 MPa [µm]**	**Fiber diameter at 36 000 rpm and 0.02 MPa [µm]**
PCL 105 °C	24 ± 12	22 ± 13
PCL 150 °C	21 ± 11	18 ± 8
PCL 200 °C	19 ± 7	14 ± 8

The effect of the melt temperature on fiber diameter is very significant as it can influence the fiber formation and solidification by different ways. Increasing the temperature allows the molten liquid jet to remain in a liquid state for longer time, thus causing the additional stretching of fiber jets. The fiber jets cool very rapidly when ejected from the orifices. Additionally, the polymer melt viscosity reduces when increasing the temperature. It has been shown that an order of magnitude reduction in shear viscosity occurs when increasing the temperature by 40 °C.[23] Therefore, thinner fibers were obtained at a higher melt temperature due to additional stretching time as well as the lower melt viscosity. It has been reported that the competition between the centrifugal force and dynamic fluid flow at the orifice against the surface tension of the polymeric solution is responsible for fiber formation in pressurized gyration.[19] This is also true in PMG where the centrifugal force accelerates the molten liquid stream and stretching of the jets. The acceleration of liquid stream and stretching is

enhanced by blowing where liquid exerts more force to overcome the surface tension force and thus results in thinner fibers at higher rotating speed and working pressure.

The surface morphology of PCL fibrous scaffolds spun at different temperatures is shown in Figure 2. Each consists of high and low magnification images. The surface of fibrous scaffolds formed at 95 and 105 °C appeared to be very smooth. The surface of the fibrous scaffolds spun at 125 °C was very rough and some particles were observed on the surface, which were probably caused by incomplete melting of polymer particles caused by nonuniform melting of the pellets during fiber forming. The fibrous scaffolds formed at higher temperatures (155 and 200 °C) show extrusion lines on the surface. These also contained fibril lines as well as small hollow regions ("pits"). The observation suggests that the melting temperature of the PCL plays a vital part in creating the surface morphology of the spun fibrous scaffolds.

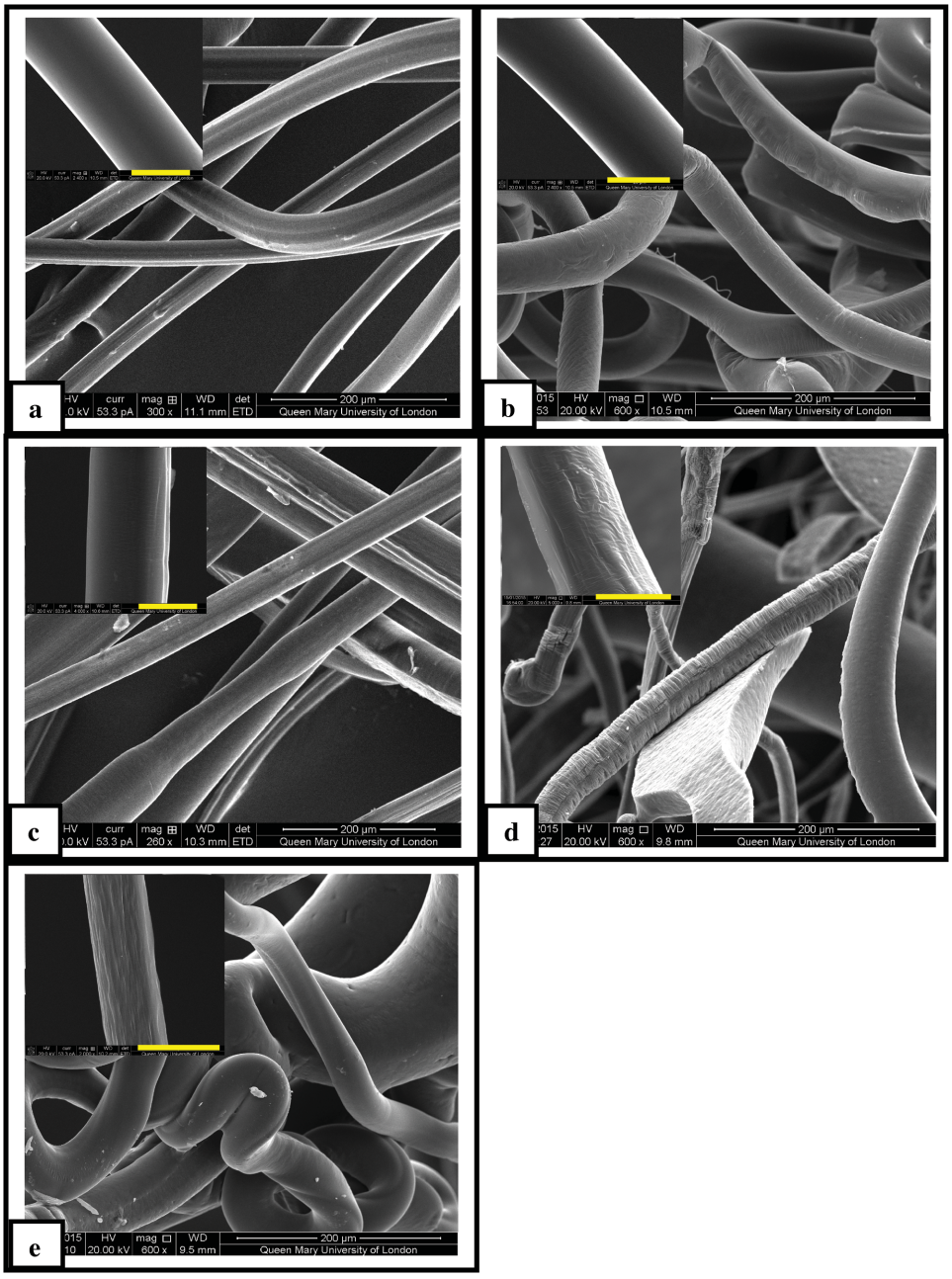

Figure 2. Scanning electron microscope images of PCL fibers obtained at various temperatures at 36 000 rpm and 0.01 MPa working pressure: a) 95, b) 105, c) 125, d) 155, e) 200 °C. Scale bars in the inset images are 20 μm.

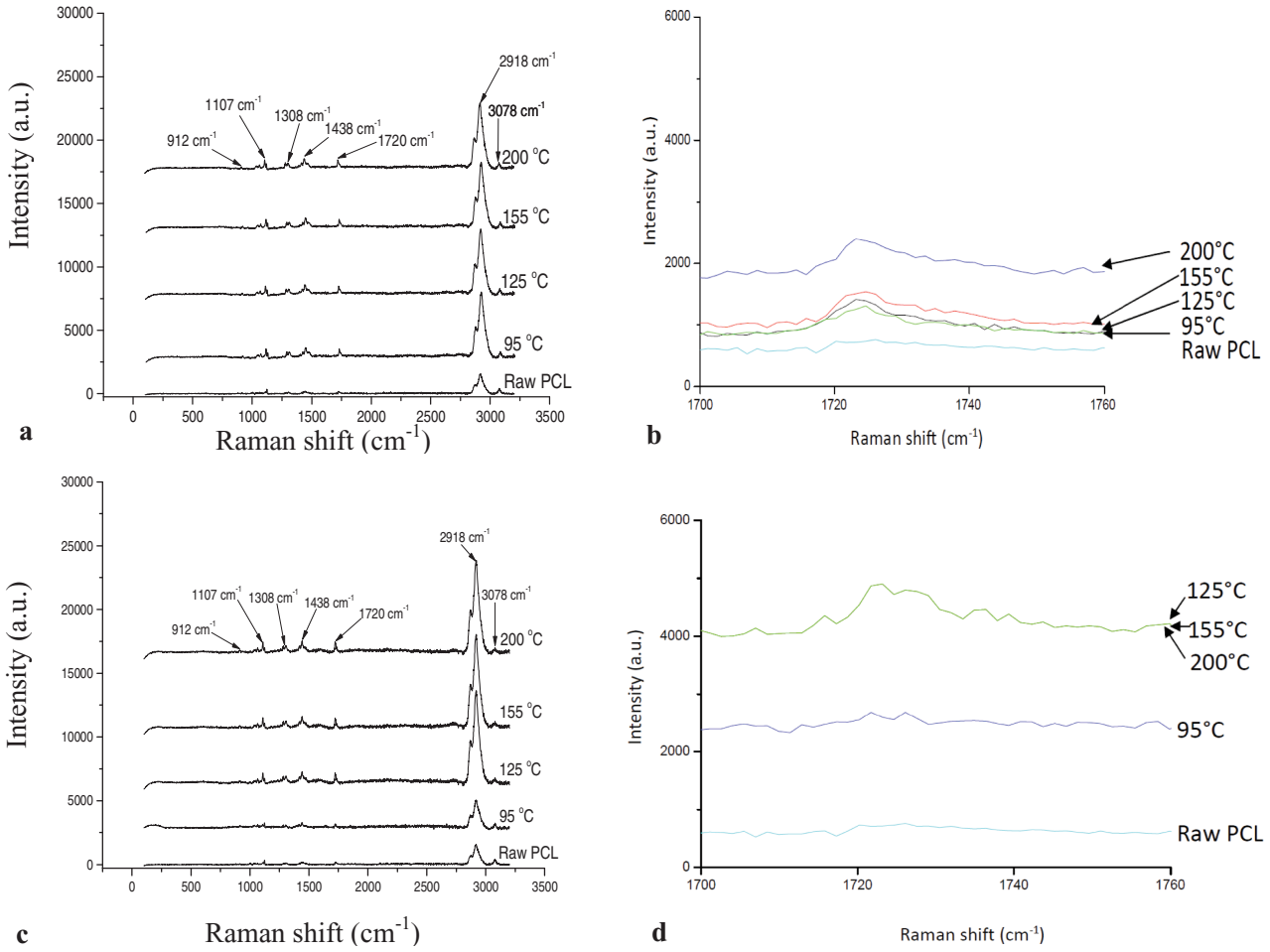

Figure 3. a) Raman spectra of PCL fibers made at various temperatures at 36 000 rpm and 0.01 MPa working pressure and raw PCL pellets. b) Microanalysis of Raman band of panel (a) in the range 1700–1760 cm^{-1}. c) Raman spectra of Ag-coated PCL fibers and raw PCL pellets. d) Microanalysis of Raman band of panel (c) in the range 1700–1760 cm^{-1}. a.u. indicates arbitrary units.

Figure 3a shows Raman spectra of PCL fibrous scaffolds obtained at various temperatures at a fixed rotating speed 36 000 rpm and 0.01 MPa working pressure. Sharp and intense peaks were observed for PCL fibrous scaffolds compared to raw PCL pellets. The intensity and the sharpness of the peaks increased with temperature, which is attributed to increase in crystallinity in the PCL scaffolds generated. The peaks at 1438, 1308, 1107, and 912 cm^{-1} correspond to (δCH_2), (wCH_2) bonding, skeletal stretching, and νC—COO bonding, respectively, and belong to crystalline phases.[24] The peak obtained between 1720–1739 cm^{-1} is assigned to C=O stretching vibration.[24] The microanalysis of the Raman band in this region is shown in Figure 3b. The PCL pellets did not reveal any peaks. However, scaffolds made at temperatures from 95 to 200 °C show a peak at ≈1723 cm^{-1} and belong to crystalline phase.[25,26] Increase of intensity and narrowing of the peak with increase in temperature indicate increase in crystallinity in the PCL scaffolds prepared. Figure 3c shows Raman spectra of Ag-coated PCL scaffolds. The main peaks identified were similar to PCL scaffolds and therefore there is not any significant difference in their molecular structure, compared to PCL scaffolds. However, the microanalysis in the wavelength range 1700–1760 cm^{-1} showed difference in their crystallinity (Figure 3d). The appearance of peaks at ≈1730 and ≈1736 cm^{-1} at higher temperatures indicates the formation of amorphous structures in the scaffolds.[25,26] This is very likely because incorporation of nanoparticles hinders the movement of molecular chains and decreases the crystallinity. It is also seen that the peak at ≈1723 cm^{-1} shifted to higher wavenumbers in the Ag-coated PCL scaffolds. This is attributed to the compressive stress present in the polymer matrix in the composite structure. It is well known that Raman peaks are associated with the lattice vibration and hence are affected by the chemical structure and

atomic bonding of the material. Therefore the stress present in the structure can affect Raman peaks.[27]

The modulated DSC results (heat–cool–heat cycle) of the PCL pellets and the fibrous scaffolds spun at different temperatures are shown in Figure 4. From the first heating scans of the products, the melting point of spun scaffolds was less than that of raw PCL pellets. The melting point of PCL pellets is 59 °C and that for the spun scaffolds lies between 57.5–59 °C and were closer to the values reported in the literature.[12] There is no apparent correlation between the melting point of scaffolds and the gyration temperatures.

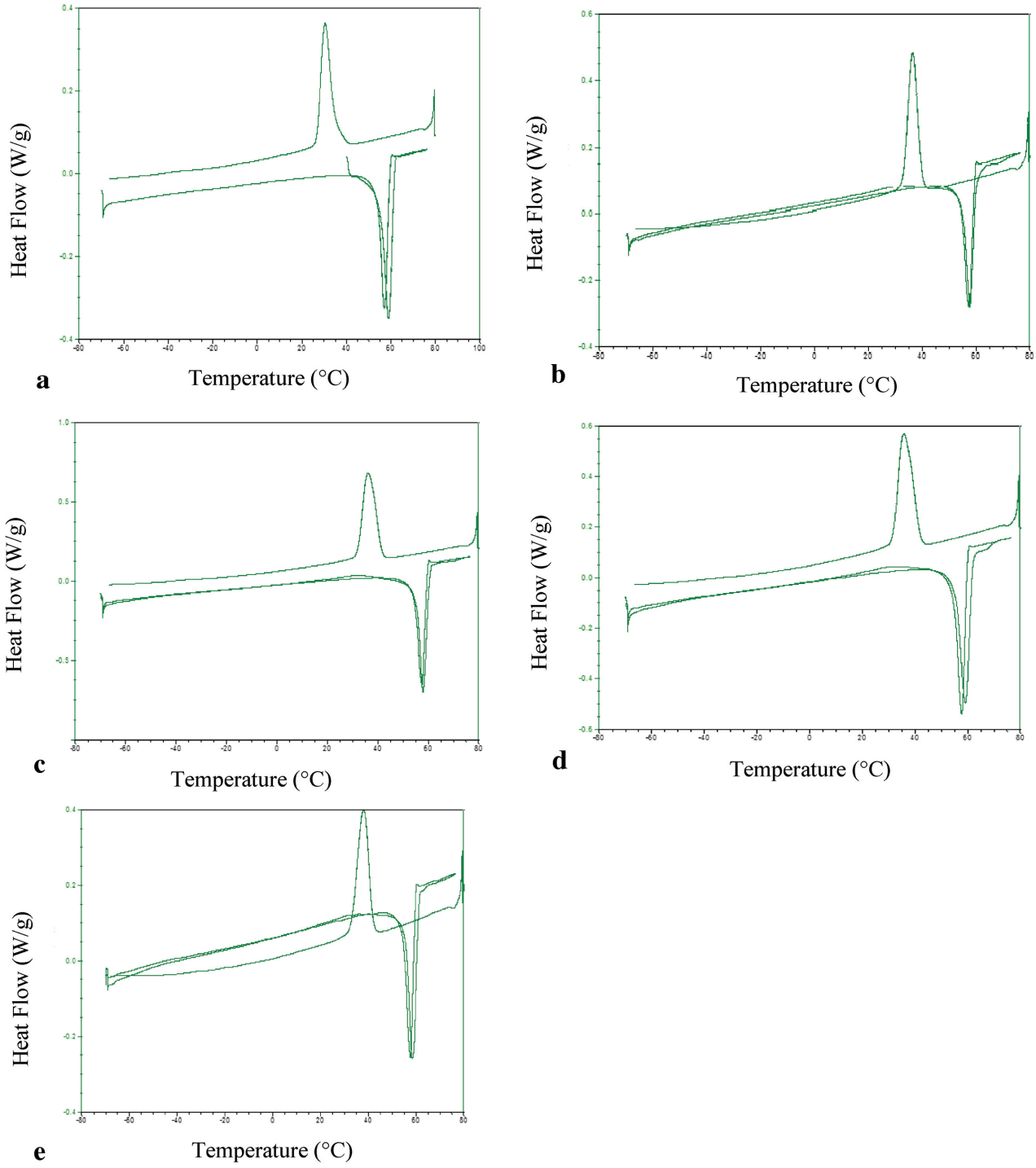

Figure 4. MTDSC results (heat–cool–heat cycle) of a) PCL pellets, fibers spun at different temperatures: b) 95, c) 125, d) 155, and e) 200 °C.

Table 2. Thermal properties of scaffolds prepared by PMG. ΔH_m, ΔH_c, T_m, T_c, and X represent melting enthalpy, crystallization enthalpy, melting temperature, crystallization temperature, and crystallinity, respectively.

Sample	ΔH_m [J g^{-1}]	ΔH_c [J g^{-1}]	T_m [°C]	T_c [°C]	X [%]
PCL pellet	–35	36	59	31	26
PCL-95 °C	–28	49	58	37	21
PCL-125 °C	–70	68	58	36	51
PCL-155 °C	–50	57	59	36	37
PCL-200 °C	–26	40	58	38	19

The thermal properties of the PCL scaffolds are summarized in Table 2. Generally, the crystallization temperature decreased with increasing melt temperature used for gyration. The crystallinity of the PCL scaffold (X%) was calculated using the equation $X\% = \Delta H_m/\Delta H_m^\circ$, where ΔH_m is the melting enthalpy taken from DSC curve and ΔH_m° is the melting enthalpy of a reference PCL with 100% crystallinity. ΔH_m° was taken as 135.6 J g^{-1}.[28] A moderate crystallinity was observed for scaffolds spun at 95 °C. Scaffolds spun at 125 °C show higher crystallinity and thereafter the crystallinity reduces with melt (gyration) temperature. This is due to variation in nucleation sites and the limited PCL molecular chain movement with the melt temperature.[29]

Silver ion (Ag^+) release profiles of different PCL-Ag fibrous scaffolds spun at different temperatures are shown in Figure 5a,b. Previous work has shown that gyration methods are able to disperse Ag nanoparticles very effectively in polymer meshes.[30] The PCL scaffold spun at 200 °C without Ag ions is also shown for comparison. The release of Ag ions from fibrous scaffolds followed an exponential increase with time, dependent on melt temperature and Ag ion content. As expected, the PCL fibrous scaffolds spun at 200 °C showed no release after 0.5–240 h. The PCL scaffolds spun at 95 °C with Ag showed low amounts of Ag ion release after 1 h. However, there was a significant amount of Ag ion release observed after 120 and 240 h. This was also true for PCL-Ag scaffolds spun at 125 °C. Although a significant amount of Ag ion release occurred in PCL-Ag scaffolds spun at higher temperatures (155 and 200 °C) throughout the release time studied, i.e., from 0.5 to 240 h, the amount of Ag ion release was almost same for both temperatures. The amount of Ag ion release from PCL scaffolds spun at higher temperatures (155 and 200 °C) started to level off and reached a plateau after 120 h in contrast to PCL scaffolds spun at lower temperatures (125 and 95 °C).

Power-law exponent, n, the slope of linear fitting between log (Ag^+) and log (t), and fitting coefficient R^2 deduced from graph in Figure 5b are shown in Table 3 and point out that n varied for the different samples, which is indicative of different transport mechanisms. For all the samples, the power-law exponent lies between ≈0.095 and 0.208 with R^2 fitting coefficient >81%. This indicates that there is no statistical correlation between the power-law exponents and the experimental measurements. Thus, these release phenomena do not closely follow $t^{1/2}$ time dependence of physical diffusion-controlled drug transport in polymer thin films based on the Higuchi model or pure Fick's second law of diffusion in a thin polymer

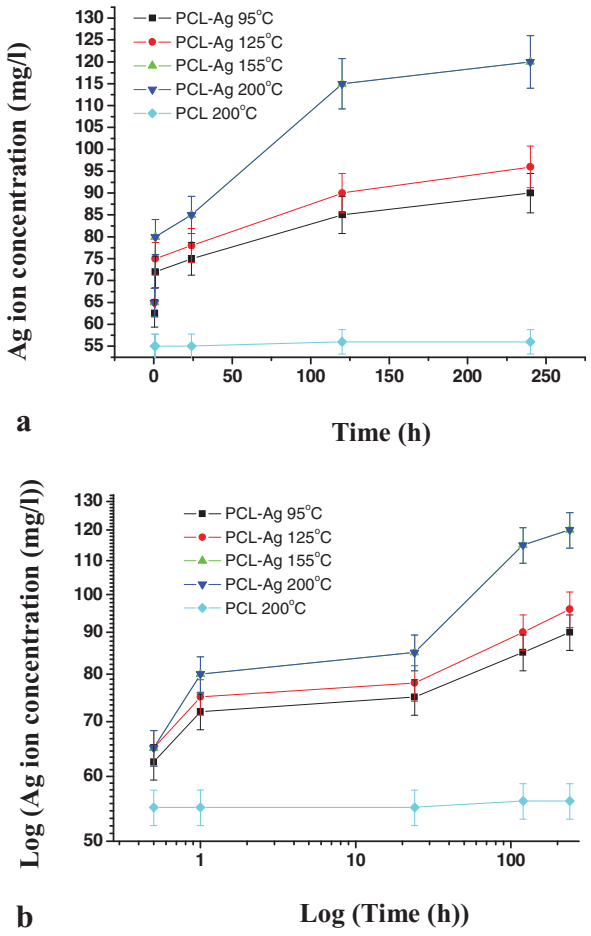

Figure 5. a) Silver ion (Ag^+) release from scaffolds in deionized water at the ambient temperature (23 °C) for various PCL fibrous scaffolds. b) Log (Ag ion concentration) versus Log (time) graphs deduced from Figure 6a.

Table 3. Release quantity of Ag^+ ions from various PCL-Ag mats in deionized water after 0.5 h, 24 h at ambient temperature (23 °C), slope of fitting and fitting coefficient of log (release quantity of Ag^+ ions) versus log (time) curve.

Sample	0.5 h Release quantity [mg L^{-1}]	24 h Release quantity [mg L^{-1}]	Slope of fitting (n)	Fitting coefficient (R^2)
PCL-200 °C	55	56	0.005	0.824
PCL-Ag 95 °C	63	90	0.095	0.814
PCL-Ag 125 °C	65	96	0.110	0.839
PCL-Ag 155 °C	65	120	0.208	0.829
PCL-Ag 200 °C	65	120	0.208	0.829

film.[31,32] The power law of Ag ion release from fibrous scaffolds spun at higher temperatures (155 and 200 °C) yields a value of 0.208, which is <0.5 with a lower R^2 fitting coefficient of 0.829. The anomalous transport of Ag ion release from the PCL fibrous scaffolds may be attributed to predominant and rapid dissolution of a large quantity of free Ag nanoparticles absorbed on the surface of fibers at the early stage of release. In addition, water permeation and crystallinity of the PCL scaffolds which constitute the diffusion barriers to water molecules and Ag ions during the propagation of release can also determine the Ag ion release rate which might contribute to the anomalous transport mechanism.[33]

Antibacterial properties of the melt spun PCL scaffolds were evaluated on Gram-negative *E. coli* and *P. aeruginosa* microorganisms. Four PCL scaffolds, four PCL-Ag coated scaffolds, and two control groups were investigated with *E. coli* and *P. aeruginosa*, respectively. Figure 6 shows the plots of antibacterial rate for *E. coli* and *P. aeruginosa* microorganisms after 2 h. It is clearly seen that the antibacterial rate for PCL-Ag coated scaffolds is higher than the PCL scaffolds for both microorganisms. The antibacterial rate of PCL scaffolds shows significant variation according to the spinning temperature used. The scaffolds spun at 200 °C show ≈40% activity, which is much higher than the other scaffolds spun at lower temperatures (95, 125, and 155 °C) for *E. coli*. Surprisingly, scaffolds spun at 95 °C show highest activity ≈70% for *P. aeruginosa*. For this microorganism, the antibacterial rate is lower for scaffolds spun at higher temperatures (125, 155, 200 °C). However, all PCL-Ag coated scaffolds showed enhanced antibacterial activity after 2 h for *E. coli*. Although the antibacterial activity of PCL-Ag coated scaffolds showed variation with spun temperatures for *P. aeruginosa*, the antibacterial activity was gradually reduced with increase in spinning temperature. It is also worth noting that there was not any antibacterial activity observed after 24 h for both microorganisms. It has been reported that Ag nanoparticle and Ag ions are responsible for bacterial cell death in Ag-coated polymer fibers.[30] Moreover, the wettability of polymer fibers increases the antibacterial activity.[34] Since PCL is hydrophobic polymer, the antibacterial activity suffers from a longer period of exposure to bacterial cells.

In vitro biocompatibility studies were carried out on the melt spun fibrous scaffolds using C2C12 myoblast cells as described in section 2.5. This cell line was chosen to investigate the potential application of these melt spun fibrous scaffolds for tissue engineering applications. The results of these biocompatibility studies have

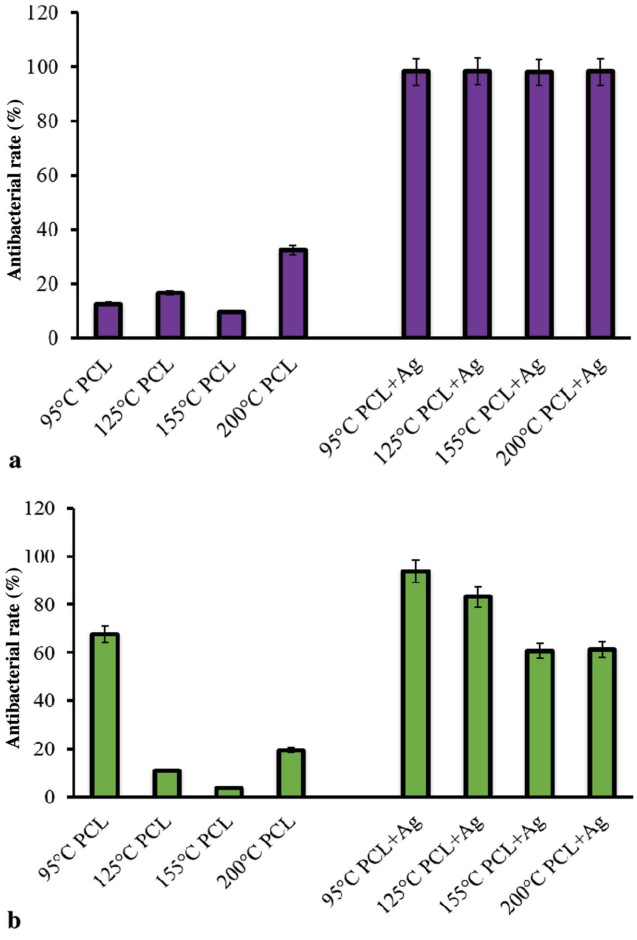

Figure 6. Antibacterial rates against a) *E. coli* after 2 h and b) *P. aeruginosa* after 2 h for different types of fiber mats prepared in this work.

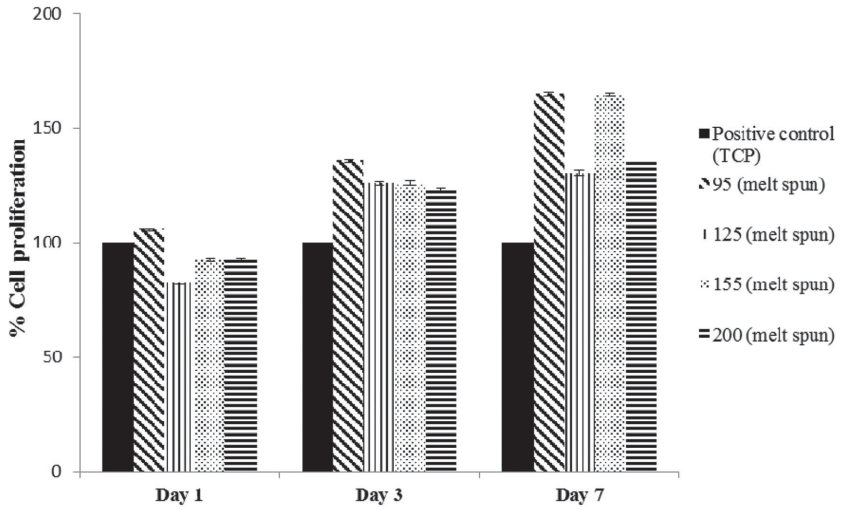

Figure 7. Cell proliferation study results using seeded C2C12 cells on the melt spun (at 95, 125, 155, and 200 °C) fibrous scaffolds on a) Day 1, b) Day 3, and c) Day 7. All the tested samples were relative to the control set at 100%.

been summarized in Figure 7. It is very clear that melt spun fibrous scaffolds were found to be biocompatible. There was no sign of any toxicity toward the C2C12 cell line. At the end of the Day 1 of cell culture, the growth of C2C12 cells on all the melt spun fibrous scaffolds was comparable to the standard tissue culture plate (positive control). Cell growth on the fibrous scaffold which was melt spun at 95 °C was higher compared to the positive control at the end of Day 1. The growth of C2C12 cells on all the melt spun fibrous scaffolds was significantly higher compared to the standard tissue culture plate at the end of Day 4. % Cell proliferation was highest on the fibrous scaffold that was melt spun at 95 °C at 136 ± 0.2%. At the

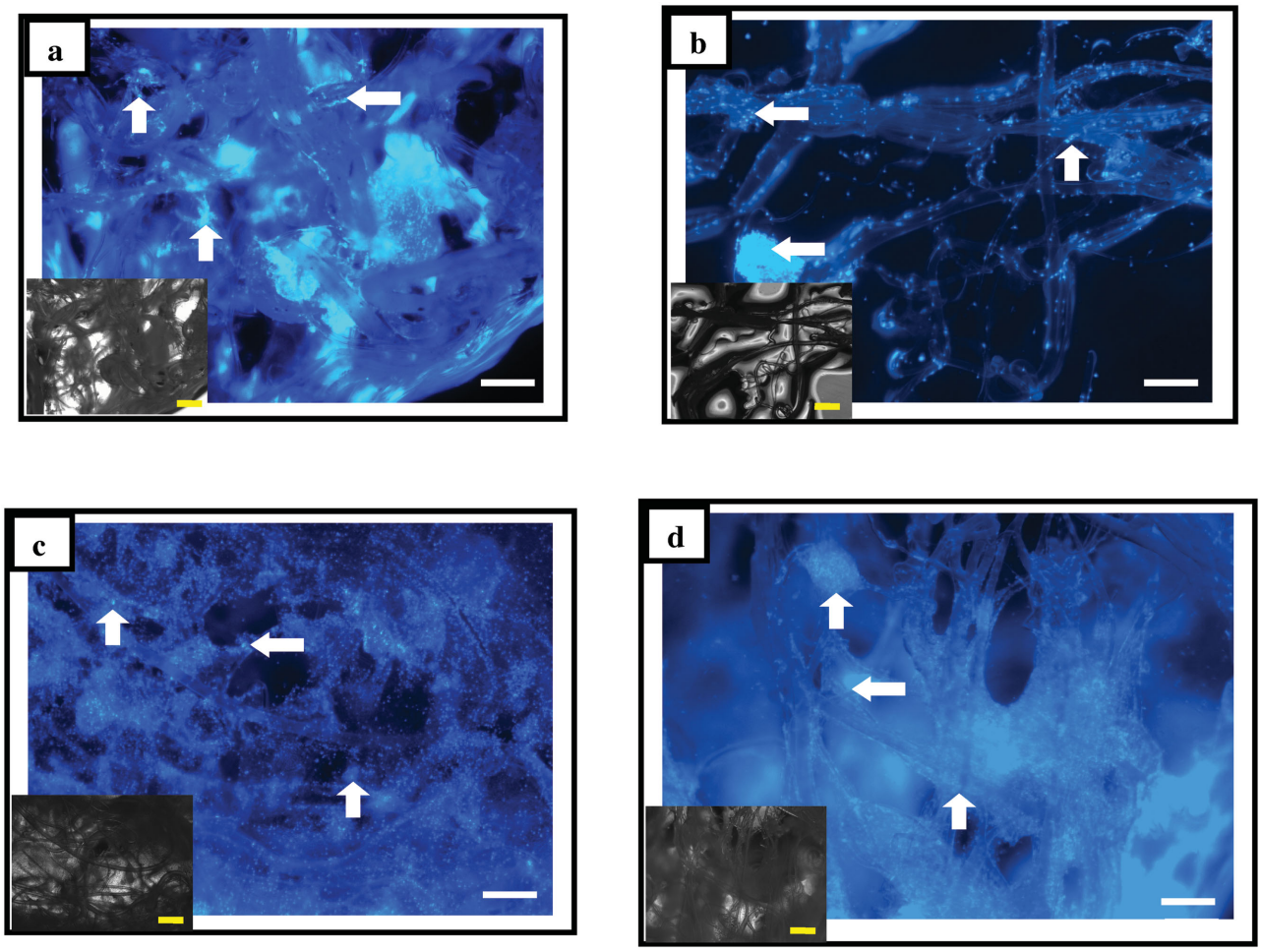

Figure 8. Stained images of different nonwoven fibrous constructs melt spun at different temperatures cultured for 1 d: a) 95, b) 125, c) 155, and d) 200 °C. Inset shows the corresponding optical images of the scaffolds. Scale bars in the images are 200 μm. Arrows in the images shows the cell nucleus and growth on fiber surface.

end of Day 7, there was a further increase in the growth of C2C12 cells on all the fibrous scaffolds compared to the cells on the standard tissue culture plate. % Cell proliferation of the C2C12 cells on the melt spun fibrous scaffolds spun at 95 and 155 °C found to be at 165.2 ± 0.3% and 165 ± 0.3%, with respect to proliferation on tissue culture plastic respectively, and those values are higher than the values obtained for other melt spun scaffolds.

Cell viability on the PCL fibrous PMG scaffolds processed at various temperatures was validated with DAPI staining to enumerate myoblast cells. Figure 8 shows the fluorescence microscopy images of the stained PCL scaffolds to highlight the cell distribution on the surface after Day 1. The scaffolds obtained at 95 °C showed higher number of attached cells compared to scaffolds obtained at 125 °C. Scaffolds obtained at 155 and 200 °C showed a higher cell attachment compared to scaffolds obtained at 125 °C. However, they showed slightly decreased numbers of attached cells compared to scaffolds generated at 95 °C. The cell attachment sites were clearly seen in the form of fibrous filaments for scaffolds obtained at 125 °C and there were distinct gaps between the attachment sites in each filament. Increased cell attachment was observed with the adjacent fibers and at point of fused fibers (Figure 8b, indicated by arrows). The cell spreading is significantly higher in the scaffolds obtained at 95 °C compared to other constructs after Day 1. Figure 9 shows the fluorescence microscopy images of the stained PCL scaffold to highlight the cell distribution on the surface after Day 7. The cell proliferation observed was extensive on all scaffold types and cell spreading was higher than Day 1. It is evident from the images that more cellular binding sites and spreading were observed for scaffolds obtained at 125 °C compared to their counterparts on Day 1. It is also clearly seen that cellular infiltration is higher in scaffolds obtained at 155 °C, where porosity within scaffolds allowed cells to infiltrate inside the scaffolds (Figure 9c). These results are consistent with the results obtained with MTT assay discussed above (Figure 7). These results also indicated that these fibrous scaffolds supported cell

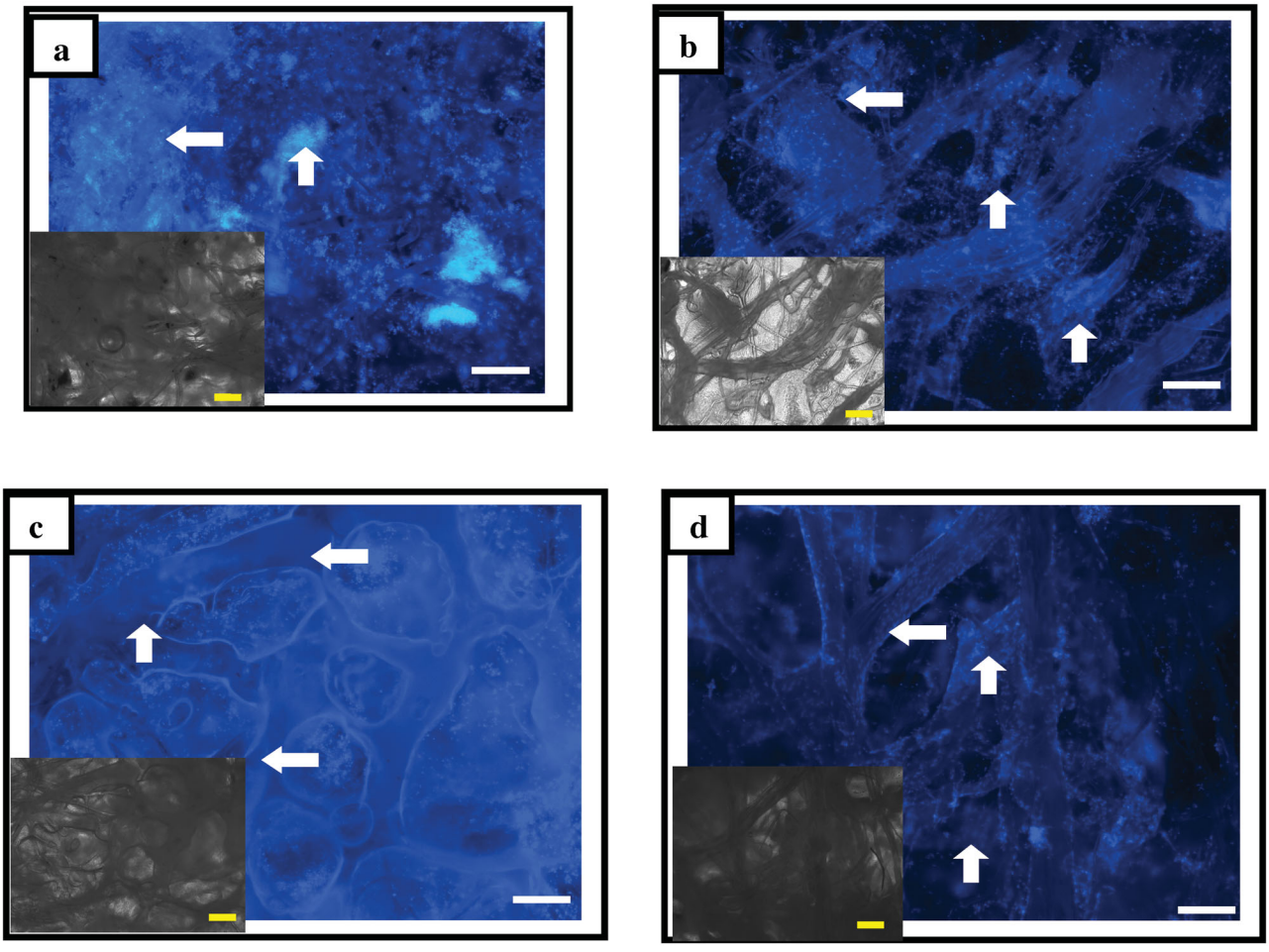

Figure 9. Stained images of different nonwoven fibrous constructs melt spun at different temperatures cultured for 7 d: a) 95, b) 125, c) 155, and (d) 200 °C. Inset shows the corresponding optical images of the constructs. Scale bars in the images are 200 μm. Arrows in the images shows cell proliferation and infiltration.

adhesion and proliferation and, therefore, they could be used as a scaffold for tissue engineering applications. Moreover, the spinning temperature and the spinning medium had an influence on the cell growth and proliferation and can be used to control cellular activity.

This study focuses on the effect of controlling the melt temperature on PCL fibrous scaffolds made using PMG and assesses the myoblast cell behavior as an indicator for muscle tissue repair and regeneration. The ECM in a tissue regulates the myoblast cell survival, differentiation, and its function. In addition, it provides the mechanical support and anchorage to the myoblast cells that sustain over the healing period of the muscle tissue.[35] The variation in cell adherence and growth for different melt gyration temperatures may be attributed to the surface morphology and the topography of the fibrous scaffolds. The cells can adhere better to smooth continuous fibers than a porous fiber surface. In addition, cells can penetrate deep inside the 3D scaffolds and protect the cells compared to a flat surface.[36] Generally, increased surface roughness promotes less cell spreading. This might be reason for less cell growth and proliferation of fibrous scaffolds spun at 125 °C.[37] Cells can easily adhere and spread on the fibrils and extruded lines that appear in the scaffolds spun at higher temperatures (155 and 200 °C). Moreover, particles can enhance performances in terms of better cell proliferation where cells can adhere more to these surface features and facilitate tissue regeneration.[38]

4. Conclusions

In this study, using PMG, PCL-based fiber nonwoven scaffolds were prepared for the first time. Rotating speed, working pressure, and temperature were very effectively used to vary the diameter, surface morphology, and the topographies of the fabricated fibrous scaffolds. The temperature significantly influenced PCL crystallinity, bonding characteristics, and Ag ion release. Antibacterial activity of the scaffolds as prepared was nearly 100% and constant for all PCL-Ag coated fibrous scaffolds for *E. coli*. The antibacterial activity gradually decreased with increase in spinning temperature for *P. aeruginosa*. Myoblast C2C12 cells showed significant attachment and growth on the fabricated scaffolds. The melt gyration temperature indirectly influenced the growth and proliferation of the cells on the scaffolds.

Supporting Information

Supporting Information is available from the Wiley Online Library or from the author.

Acknowledgements: The authors are grateful to the EPSRC funding (EP/L023059/1) which partly supported this work. The authors are very grateful to Dr. Jennifer Rohn from Centre for Clinical Science and Technology, Division of Medicine, University College London for allowing Zewen to use her experimental facilities for antibacterial studies. Queen Mary, University of London is thanked for use of electron microscopy facilities. Data supporting this study are provided in the paper and as Supporting Information accompanying this paper.

Received: March 7, 2016; Revised: March 20, 2016; Published online: May 2, 2016; DOI: 10.1002/mame.201600116

Keywords: antibacterial; constructs; fibers; gyration; melt; nonwoven; polymer; pressure; tissue engineering

[1] M. van Lieshout, G. Peters, M. Rutten, F. Baaijens, *Tissue. Eng. Part A* **2006**, *12*, 481.
[2] D. Li, T. Wu, N. He, J. Wang, W. Chen, L. He, C. Huang, H. A. El-Hamshary, S. S. Al-Deyab, Q. Ke, *Colloid Surf., B* **2014**, *121*, 432.
[3] G. Narayanan, B. S. Gupta, A. E. Tonelli, *Biomacromolecules* **2014**, *15*, 4122.
[4] J. Ren, K. A. Blackwood, A. Doustgani, P. P. Poh, R. Steck, M. M. Stevens, M. A. Woodruff, *J. Biomed. Mater. Res., Part A* **2014**, *102*, 3140.
[5] D. Sankar, K. T. Shalumon, K. P. Chennazhi, D. Menon, R. Jayakumar, *Tissue Eng., Part A* **2014**, *20*, 1689.
[6] W. Liu, S. Thomopoulos, Y. Xia, *Adv. Healthcare Mater.* **2012**, *1*, 10.
[7] V. Beachley, E. Katsanevakis, N. Zhang, X. Wen, *Adv. Healthcare Mater.* **2013**, *2*, 343.
[8] J. Ko, N. K. Mohtaram, F. Ahmad, A. Montgomery, M. Carlson, P. C. D. Lee, S. M. Willerth, M. B. G. Jun, *J. Biomater. Sci.* **2014**, *25*, 1.
[9] T. D. Brown, F. Edin, N. Detta, A. D. Skelton, D. W. Hutmacher, P. D. Dalton, *Mater. Sci. Eng. C* **2014**, *45*, 698.
[10] S. J. Park, B-K. Lee, M. H. Na, D. S. Kim, *Acta Biomater.* **2013**, *9*, 7719.
[11] N. K. Mohtaram, J. Ko, C. King, L. Sun, N. Muller, M. B. Jun, S. M. Willerth, *J. Biomed. Mater. Res., Part A* **2015**, *103*, 2591.
[12] S. Jana, M. Leung, J. Chang, M. Zhang, *Biofabrication* **2014**, *6*, 035012.
[13] O. Catanzano, S. Acierno, P. Russo, M. Cervasio, M. D. B. De Caro, A. Bolognese, G. Sammartino, L. Califano, G. Marenzi, A. Calignano, D. Acierno, F. Quanglia, *Mater. Sci. Eng C* **2014**, *43*, 300.
[14] F. Croisier, G. Atanasova, Y. Poumay, C. Jerome, *Adv. Healthcare Mater.* **2014**, *3*, 2032.
[15] Z. Wang, Y. Cui, J. Wang, X. Yang, Y. Wu, K. Wang, X. Gao, D. Li, Y. Li, X-L. Zheng, Y. Zhu, D. Kong, *Biomaterials* **2014**, *35*, 5700.
[16] S. Gea, C. T. Reynolds, N. Roohpur, N. Soykeabkaew, B. Wirjosentono, E. Bilotti, T. Peijs, *J. Biobased Mater. Bioenergy* **2010**, *4*, 384.
[17] H.-Y. Mi, X. Jing, J. Peng, M. R. Salick, X.-F. Peng, L.-S. Turng, *Cellulose* **2014**, *21*, 2727.
[18] R. Augustine, H. N. Malik, D. K. Singhal, A. Mukherjee, D. Malakar, N. Kalarikkal, S. Thomas, *J. Polym. Res.* **2014**, *21*, 347.
[19] S. Mahalingam, M. Edirisinghe, *Macromol. Rapid Commun.* **2013**, *34*, 1134.

[20] B. T. Raimi-Abraham, S. Mahalingam, M. Edirisinghe, D. Q. M. Craig, *Mater. Sci. Eng C* **2014**, *39*, 168.
[21] S. Mahalingam, G. G. Ren, M. Edirisinghe, *Carbohydr. Polym.* **2014**, *114*, 279.
[22] S. Mahalingam, B. T. Raimi-Abraham, D. Q. M Craig, M. Edirisinghe, *Langmuir* **2015**, *31*, 659.
[23] J. Vera-Sorroche, A. L. Kelly, E. C. Brown, T. Gough, C. Abeykoon, P. D. Coates, J. Deng, K. Li, E. Harkin-Jones, M. Price, *Chem. Eng. Res. Des.* **2014**, *92*, 2404.
[24] K. K. Gupta, A. Kundan, P. K. Mishra, P. Srivastava, S. Mohanty, N. K. Singh, A. Mishra, P. Maiti, *Phys. Chem. Chem. Phys.* **2012**, *14*, 12844.
[25] G. Kister, G. Cassanas, M. Bergounhon, D. Hoarau, M. Vert, *Polymer* **2000**, *41*, 925.
[26] O. Hartman, C. Zhang, E. L. Adams, M.-C. Farach-Carson, N. J. Petrelli, B. D. Chase, J. F. Rabolt, *Biomaterials* **2010**, *31*, 5700.
[27] D. Lahiri, F. Rouzaud, T. Richard, A. K. Keshri, S. R. Bakshi, L. Kos, A. Agarwal, *Acta Biomater.* **2010**, *9*, 3524.
[28] C. J. Ong, F. P. Price, *J. Polym. Sci., Polym. Symp.* **1978**, *63*, 45.
[29] J.-Z. Liang, L. Zhou, C.-Y. Tang, C.-P. Tsui, *J. Appl. Polym. Sci.* **2013**, *128*, 2940.
[30] Z. Xu, S. Mahalingam, J. L. Rohn, G. Ren, M. J. Edirisinghe, *Mater. Sci. Eng. C* **2015**, *56*, 195.
[31] D. R. Paul, *Int. J. Pharm.* **2011**, *418*, 13.
[32] J. Siepmann, N. A. Peppas, *Int. J. Pharm.* **2011**, *418*, 6.
[33] C. Radheshkumar, H. Munstedt, *React. Funct. Polym.* **2006**, *66*, 780.
[34] K.-H. Jung, M.-W. Huh, W. Meng, J. Yuan, S. H. Hyun, J.-S. Bae, S. M. Hudson, I.-K. Kang, *J. Appl. Polym. Sci.* **2007**, *105*, 2816.
[35] S. Sahoo, S. L. Toh, J. C. H. Goh, *Biomaterials* **2010**, *31*, 2990.
[36] S. Francois, N. Chakfe, B. Durand, G. Laroche, *Acta Biomater.* **2009**, *5*, 2418.
[37] O. Zinger, K. Anselme, A. Denzer, P. Harbersetzer, M. Wieland, J. Jeanfils, P. Hardouin, D. Landolt, *Biomaterials* **2004**, *25*, 2695.
[38] L. Francis, J. Venugopal, M. P. Prabhakaran, V. Thavasi, E. Marsano, S. Ramakrishna, *Acta Biomater.* **2010**, *6*, 4100.